Effects of capacitors, resistors and residual charge on the static and dynamic performance of electrostatically-actuated devices

E. K. Chan and R.W. Dutton
CISX 305, Center for Integrated Systems
Stanford University
Stanford, CA 94305-4075, USA

ABSTRACT

The important practical and realistic design issues of an electrostatic actuator/positioner with full-gap travel are discussed. Analytic expressions and numerical simulations show that parasitic capacitances, and non-uniform deformation in two and three dimensions influence the range of travel of an electrostatic positioner stabilized by the addition of a series capacitor. The effects of residual charge on electrostatically-actuated devices are described. The dynamic stepping characteristics of the positioner under compressible squeeze-film damping and resistive damping are compared. The physical descriptions of devices being fabricated in the MUMPs process are presented along with 3D simulation results that demonstrate viability.

Keywords: electromechanical, full-gap travel, stable, folded capacitor, floating electrode, shielded tether

1. INTRODUCTION

Electrostatically-actuated devices are widely used in microelectromechanical systems as switches [1] and resonators [2], and to extract material properties [3]. A typical device of this nature consists of a movable electrode suspended over a fixed electrode (Fig. 1a). An electric field imposed by applying a voltage between the electrodes actuates the movable electrode towards the fixed electrode. At voltages above a critical voltage known as the "pull-in voltage", the movable electrode collapses onto the fixed electrode. This restricted range of stable travel – about one-third of the initial gap – limits the effectiveness of electrostatic actuators as analog positioners. Several methods to extend the usable range of travel have been proposed such as employing "leveraged bending" [4], closed-loop voltage control [5], and series feedback capacitance [6].

The practical and realistic issues involved in designing a full-gap positioner by adding a capacitor in series with the electrostatic actuator – which is essentially a variable capacitor – to stabilize the actuator are presented in detail in subsequent sections. It is shown that parasitic elements inherent in fabricated devices, and any deviation from ideal 1D behavior limit the stable travel range. Residual charge that can accumulate in dielectrics and electrically-isolated nodes cause a voltage offset in this positioner. The stepping characteristics of this actuator/positioner under compressible squeeze-film damping and resistive damping are compared. Over-stabilization speeds up rise times without increasing settling times. Finally, the physical design of an electrostatic positioner, employing a novel floating electrode, that is currently being fabricated in the MUMPs process (MUMPs) [7] of the Microelectronics Center of North Carolina (MCNC) is described. This device which we call a "folded capacitor" actuator incorporating shielded tethers meets the design requirements for full-gap positioning.

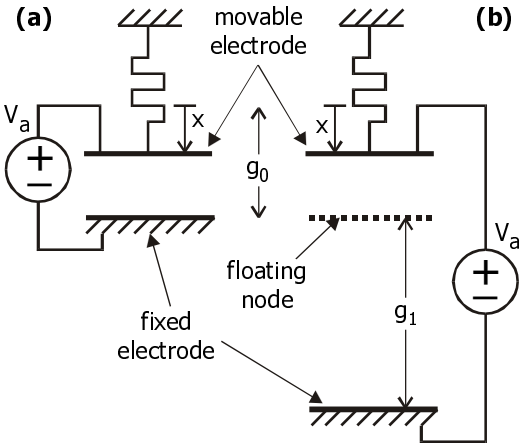

Fig. 1. (a) *Schematic representation of conventional electrostatically-actuated device consisting of a movable electrode suspended over a fixed electrode.* ***(b)*** *Schematic representation of electrostatic positioner with series capacitor stabilization. The series capacitor increases the total effective gap between the voltage-driven electrodes. The floating node partitions the gap into the two capacitors -- the actuator and series capacitor..*

2. BEHAVIOR OF CONVENTIONAL ACTUATOR

Fig. 1a is a schematic representation of a typical electrostatically-actuated device consisting of a movable top electrode suspended over a fixed bottom electrode. An electrostatic force set up by applying a voltage between the top and bottom electrodes pulls the top electrode towards the bottom. Considering an ideal one-dimensional (1D) system with electrodes of unit area, the equilibrium position of the movable electrode is determined by equating a mechanical restoring force of

$$F_m = -kx \tag{2.1}$$

with an attractive electrostatic force of

$$F_e = \frac{\varepsilon V_a^{\,2}}{2(g_0 - x)^2} \tag{2.2}$$

where k is the mechanical spring constant, x is the displacement of the top electrode, ε is the dielectric permittivity of the region between the electrodes, V_a is the applied voltage, and g_0 is the initial (unactuated) gap between the electrodes. Analytic calculations show that beyond

$$V_a = \sqrt{\frac{8kg_0^{\,3}}{27\varepsilon}} \tag{2.3}$$

corresponding to a displacement of

$$x = \frac{1}{3} g_0 \tag{2.4}$$

there is no equilibrium position for the top electrode, which hence collapses onto the bottom electrode. Therefore, the stable range of travel is limited.

3. SERIES CAPACITOR FEEDBACK

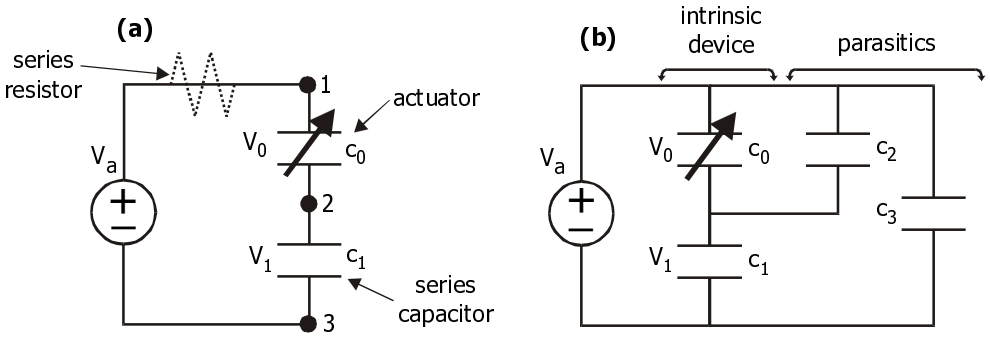

Fig. 2. (a) *Circuit diagram of stabilized electrostatic positioner. Voltage across the actuator is determined by the capacitive voltage divider. Series resistor can be included to provide resistive damping.* ***(b)*** *Circuit diagram including parasitic capacitances. Voltage across actuator is given by Eq. 3.4. Capacitor c_3 only affects dynamic performance.*

3.1 Ideal behavior

A properly-sized capacitor added in series with the conventional actuator will adjust the actual voltage between the electrodes of the actuator so that the movable electrode can traverse the entire gap stably [6]. The capacitive voltage divider of Fig. 2a suggests that the total applied voltage, V_a, is divided between the actuator and the series capacitor such that

$$V_0 = \frac{c_1}{c_0 + c_1} V_a \,. \tag{3.1}$$

Since the capacitance of the actuator, c_0, increases as the movable electrode approaches the fixed electrode, the fraction of the applied voltage across the actuator actually decreases as the applied voltage is increased. When the displacement extends beyond one-third of the gap, the rapid increase in capacitance provides the negative feedback necessary to stabilize the actuator so it can traverse the entire gap stably.

This behavior can equivalently and more easily be understood as actuating the movable electrode through the stable range of an actuator with a larger effective initial gap, $g_0 + g_1$, as shown in Fig. 1b. The series capacitor of Fig. 2a serves to increase the total effective gap of the actuator such that the movable electrode moves only through the stable portion of the gap. A floating conductor inserted at the dotted line in Fig. 1b partitions the system into two capacitors in series without disturbing the field distributions. Since the stable range is one-third of the total effective gap, g_1 needs to be at least twice as large as g_0 to achieve stable full-gap travel. In terms of capacitances, this condition is

$$c_1 < \frac{c_0^i}{2} \tag{3.2}$$

where c_0^i is the initial actuator capacitance.

3.2 Effect of parasitics

Fig. 3 shows the cross-section of a typical electrostatically-actuated device fabricated in the MUMPs process. c_0 and c_1 are the intrinsic device capacitances whereas c_{p1}, c_{p2} and c_{p3} are parasitics. c_{p2} and c_{p3} are typically large because the dielectric layer is (electrically) thin. Depending on whether the substrate is grounded or left floating, the parasitic capacitances can be in parallel with either c_0 or c_1. The circuit of Fig. 2a can be generalized to that shown in Fig. 2b where c_1 now includes the parasitics in parallel with it. c_3 is not important to the static solution since it is driven directly by the voltage source, but it will affect dynamic performance.

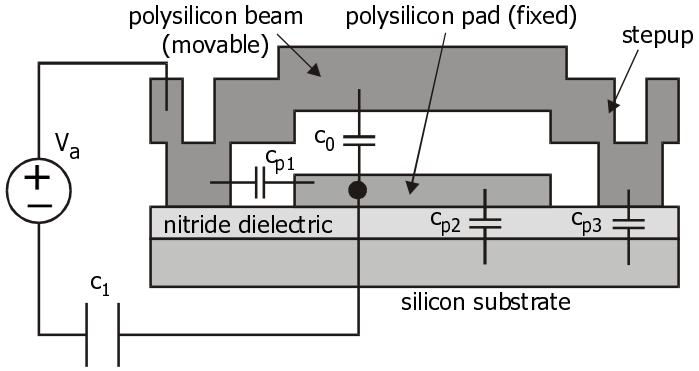

Fig. 3. *Profile of typical electrostatically-actuated device fabricated in MUMPs. Parasitic capacitances to the substrate are typically large because the nitride is thin. Displacement is largest at the center of the beam. The length of the fixed bottom pad can be reduced to influence primarily the center portion of the beam thus approaching 1D behavior.*

We now derive expressions describing the static behavior of the actuator in the presence of a series feedback capacitor and parasitic capacitors as depicted in Fig. 2b. Let

$$c_0 \propto \frac{1}{g_0 - x},\ c_1 \propto \frac{1}{ng_0} \text{ and } c_2 \propto \frac{1}{mg_0} \tag{3.3}$$

where m and n are positive constants. The voltage across c_0 is determined by the capacitive voltage divider to be

$$\begin{aligned} V_0 &= \frac{c_1}{c_0 + c_1 + c_2} V_a \\ &= \frac{m(g_0 - x)}{(m+n)(g_0 - x) + mng_0} V_a \end{aligned} . \tag{3.4}$$

The sum of the electrostatic and mechanical forces gives the total equilibrium force on the movable electrode

$$F_t = -kx + \frac{\varepsilon}{2(g_0 - x)^2}\left[\frac{m(g_0 - x)}{(m+n)(g_0 - x) + mng_0} V_a\right]^2 = 0 . \tag{3.5}$$

Differentiating this expression with respect to x to determine the point at which the equilibrium solution becomes unstable gives

$$x_{\max} = \frac{g_0}{3}\frac{m+n+mn}{m+n} \tag{3.6}$$

as the maximum stable displacement of the movable electrode as a function of m and n. In the limit as $m \to \infty$ (no parasitic fixed capacitor in parallel with c_0),

$$x_{\max} \to \frac{g_0}{3}(1+n) \tag{3.7}$$

implying that n should be larger than 2 for full-gap travel ($x_{\max} \to g_0$) as noted previously. As $n \to \infty$ (infinitely small series capacitor for maximum stability),

$$x_{\max} \to \frac{g_0}{3}(1+m) \tag{3.8}$$

implying that c_2 must be no larger than $\frac{c_0^i}{2}$ if full-gap travel is to be achieved. Thus the electrostatic positioner must have well-controlled capacitances and parasitics.

4. DEFORMATION IN TWO-DIMENSIONS

When the beam in Fig. 3 deforms, the displacement of the center portion is largest whereas the portions near the stepup supports hardly move at all. This 2D non-uniform behavior is a subtle but significant source of "parasitic" capacitance, c_2, in parallel with c_0. The 2D beam/capacitor can be modeled as the sum, of two 1D capacitances – a variable capacitor in parallel with a fixed capacitor as shown in Fig. 4. This is expressed as

$$c = c_0 + c_2 \propto \frac{1-q}{g_0 - x} + \frac{q}{g_0} \tag{4.1}$$

where c_0 and c_2 represent the same elements as in Fig. 2b, and q is a proper fraction that increases as x, the center displacement, increases as will be shown later. The larger the value of q, the larger the effect of the parasitic.

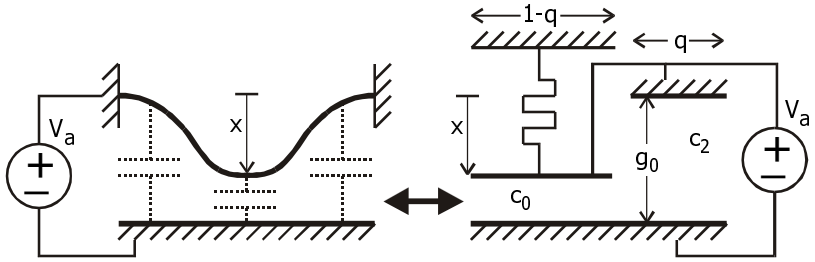

Fig. 4. *Ideal 2D electrostatically-actuated beam with its lumped-element representation that is parameterized by the center displacement of the beam, and the fraction "q" of the beam that behaves like a parasitic parallel fixed capacitance.*

Fig. 5a shows the normalized simulated capacitances of several 2D 400μm-long electrostatically-actuated beams, with nominal MUMPs thicknesses, as functions of the displacement of the beam center. The coupled electromechanical simulations were performed in Matlab [8]. As shown, the capacitance of a 2D device increases more slowly as a function of center displacement than a 1D device. Numerical experiments show that the normalized capacitance is relatively insensitive to beam length and residual stress. As the fixed bottom electrode on the left-hand side of Fig. 4 is reduced in length (as a percentage of the upper beam length), the 2D device approaches 1D-like behavior because the deformation is more uniform over the more limited center region.

q is computed from the capacitance-displacement curves of Fig. 5a and plotted in Fig. 5b as a function of center displacement, x, and parameterized by bottom electrode length. The shorter the bottom electrode, the more 1D-like the behavior, hence the smaller the value of q. q increases as the displacement increases because the smaller gap amplifies the

effect of non-uniform displacements. Since c_2 must be less than one-half the initial c_0 for full-gap actuation as shown in Section 3, q must satisfy

$$\frac{q}{g_0} < \frac{1-q}{2g_0} \Leftrightarrow q < \frac{1}{3}. \tag{4.2}$$

The displacement at the intersection of the $q = 1/3$ line with the q-displacement curve indicates the maximum achievable stable travel. This assumes that the mechanical restoring force is still linear with displacement, which is not strictly true due to stress-stiffening effects. Nonlinear stress-stiffening actually increases the range of stable travel, even without capacitive stabilization, to about one-half the initial gap, up from the one-third (Eq. 2.4) of the linear case. Thus all the 2D devices shown in Fig. 5b are stable up to about 1μm of deflection. Beyond that, capacitive feedback can stabilize the device up until the increasing displacement causes $q > 1/3$. For example, for the device with a bottom electrode that is 30% of the upper electrode length, capacitive feedback will allow stable travel up to 1.8μm or 90% of the 2μm gap. This, however, assumes an infinitely small series feedback capacitor (see Eq. 3.8) – a larger capacitor will reduce the travel range. Clearly, 2D-like behavior must be avoided.

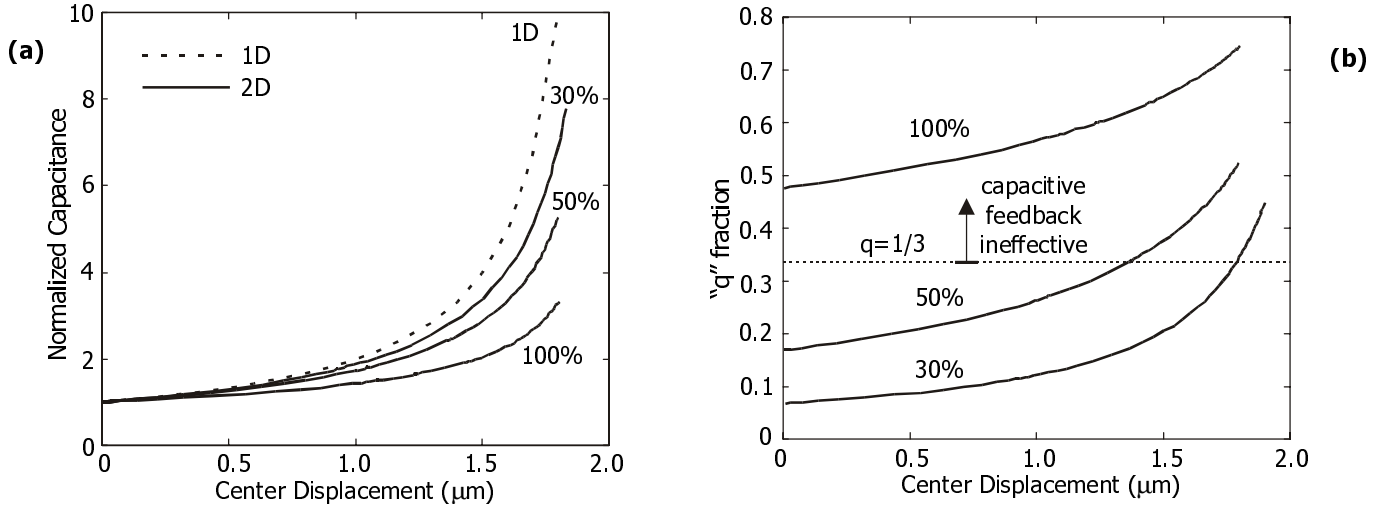

Fig. 5. (a) *Normalized simulated capacitances of 2D 400μm-long electrostatically-actuated beams as functions of center displacement and parameterized by bottom electrode length (as a percentage of upper beam length). The increase in capacitance in the 2D case is always less than in 1D. As the fixed bottom electrode length is reduced from 100% of beam length to 30%, the capacitance variation approaches 1D behavior.* ***(b)*** *The fraction "q" of the 2D beam that behaves like a parasitic fixed capacitance in parallel with the variable capacitance. q increases with displacement because the decreasing gap accentuates the effect of non-uniform displacement along the length of the beam. The dotted line where q=1/3 is the boundary above which capacitive feedback is ineffective. Due to stress-stiffening, the center of the 2D beams can move almost 1μm before pull-in occurs even without capacitive feedback.*

Referring back to Fig. 1b, we see that in the 1D case, inserting a floating conductor into the gap at the dotted line does not perturb the electric field lines. When a 2D beam deforms non-uniformly, however, the beam center moves the most, concentrating electrostatic forces near the center. Inserting a floating conductor into the gap in this case will distort the electric field lines since the conductor will enforce a flat, horizontal equipotential which did not previously exist. The series capacitor no longer simply extends the effective gap and thus the effectiveness of capacitive feedback is limited. Designs to maintain 1D-like behavior are discussed in Section 7.

5. RESIDUAL CHARGE

Residual charge can accumulate in electrostatically-actuated devices containing electrically-isolated nodes or dielectric layers. Fig. 6 shows the effect of a sheet of charge inserted between two voltage-driven plates. Both trapped charge in a dielectric layer [3], or net charge on a floating node such as node 2 in Fig. 2a can be modeled by a sheet of charge. According to Gauss' Law, the charge sheet modifies the electric field on each side of the sheet to be

$$E_1 = \frac{V_a - \frac{d_2 \rho}{\varepsilon}}{d_1}, \text{ and} \tag{5.1}$$

$$E_2 = \frac{V_a + \frac{(d_1 - d_2)\rho}{\varepsilon}}{d_1} \tag{5.2}$$

where ρ is the areal charge density of the charge sheet. For most electrostatically-actuated devices, the movable electrode is plate 1 in Fig. 6. In this case, the electric field, and hence the electrostatic force, is simply shifted by a voltage offset ($\frac{d_2 \rho}{\varepsilon}$ in Eq. 5.1) which scales according to the amount of charge.

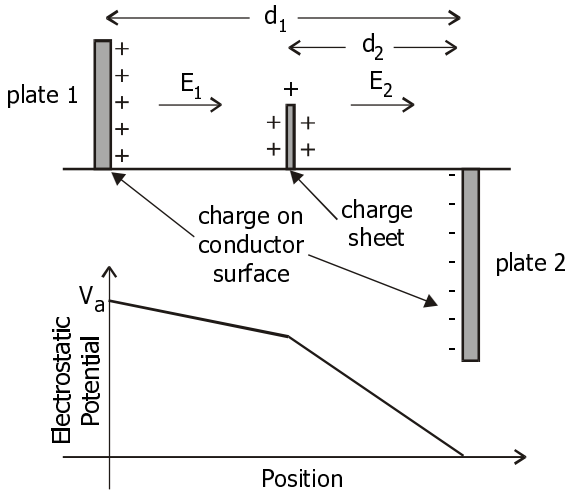

Fig. 6. *Effect of residual charge, represented by a sheet of charge, on the electrostatics between two voltage-driven plates. The slope of the electrostatic potential changes abruptly at the position of the charge sheet.*

If the electric field on both sides of the charge sheet act on movable electrodes, however, the effect is more complicated. Fig. 7a shows one such configuration where a precharged floating conductor inserted between two voltage-driven plates is free to move. The mechanical restoring force is still given by Eq. 2.1 but the electrostatic force – the product of charge and the average electric field – is now

$$F_e = \rho \left[\frac{V_a}{d_1} - \frac{\rho}{\varepsilon} \left(\frac{d_2 - x}{d_1} - \frac{1}{2} \right) \right]. \tag{5.3}$$

The first thing to note is that unless the floating conductor is precharged, the net electrostatic force on the conductor is zero. Secondly, in contrast to Eq. 2.2, this force is linear with voltage and displacement. By equating the electrostatic and mechanical forces, we find the equilibrium displacement to be

$$x = \frac{\frac{V_a}{d_1} - \frac{\rho}{\varepsilon} \left(\frac{d_2}{d_1} - \frac{1}{2} \right)}{\frac{k}{\rho} - \frac{\rho}{\varepsilon d_1}}. \tag{5.4}$$

Here, the charge scales not just the voltage offset but the displacement axis as well. Since the inverse-square behavior of Eq. 2.2 is absent, there is no abrupt pull-in effect and actuation is always stable, potentially allowing for stable and linear electrostatic actuation. Figs. 7b and 7c are the layout and cross-section of a proposed implementation of this linear actuator being fabricated in MUMPs. The POLY1 floating electrode is suspended by flexible tethers with meanders so that it can move easily within the gap. On the other hand, the POLY2 electrode is designed to be short to minimize its undesired deformation under electrostatic forces. The floating electrode is precharged by briefly connecting it to a voltage source. Like

the capacitively-stabilized actuator, the performance of this actuator is affected by parasitic capacitances. Good isolation of the floating conductor and matching electrode areas is critical for linearity. This, unfortunately, is difficult to achieve in MUMPs.

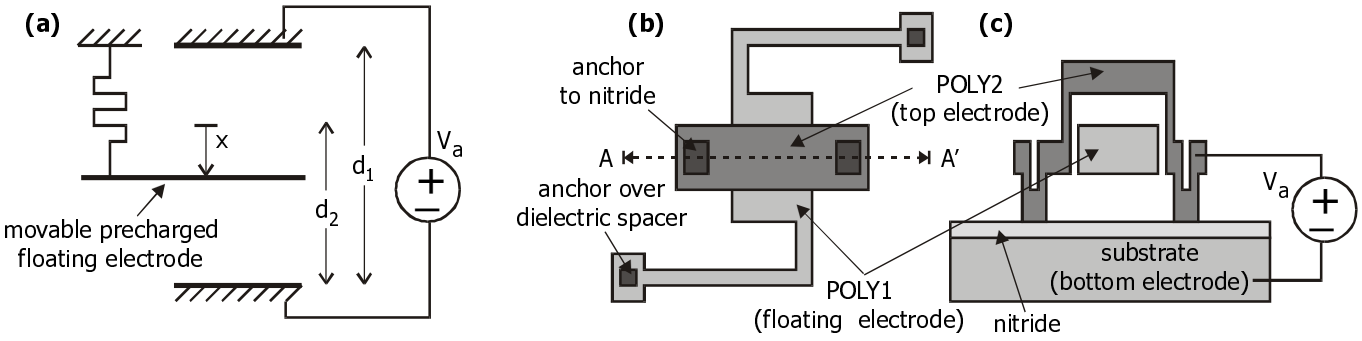

Fig. 7. *Linear electrostatic actuator consisting of a movable precharged floating electrode suspended between two voltage-driven electrodes. Displacement is proportional to applied voltage and depends on precharge voltage.* ***(a)*** *Schematic representation.* ***(b)*** *Layout of proposed device being fabricated in MUMPs. The top POLY2 electrode is designed to be short so as not to deform easily. The POLY1 floating electrode, on the other hand, is suspended by flexible tethers so that it can be actuated.* ***(c)*** *Cross-section AA' corresponding to layout (b). Actuation voltage, V_a, is applied between substrate and POLY2 electrode. Precharge voltage is applied briefly to floating electrode.*

6. DAMPING

A good positioner or actuator should be well-damped so that rise times are fast, settling times are short, and overshoots are small. The efficacy of the two common damping mechanisms for microelectromechanical devices – resistive damping and compressible squeeze-film damping – on stabilized electrostatic positioners are studied using 1D simulations. The simulation models used here are not calibrated to actual devices but serve to illustrate major damping characteristics. For conventional actuators (see Section 2), the only dynamic responses of interest are pull-in and release times since these devices are usually operated in on/off modes, and involve contact [8]. For analog positioners, however, the dynamic response from one position to another throughout the gap is of interest.

A resistor inserted in series with the voltage source in Fig. 2a will help damp out oscillatory behavior by dissipating energy when current flows. Fig. 8a is an example of the damped step responses of an ideal, 1D, critically-stabilized positioner ($c_1 = \frac{c_0^i}{2}$). The resistor damps out oscillations reasonably well for steps down from $x = 0$, especially for larger steps ($x > 0.5g_0$). The size of the resistor was chosen so that the overshoot for the $x = 0.9g_0$ step would not cause the movable electrode to make contact and possibly stick to the bottom electrode. The resistor performs poorly in damping out the oscillations stepping back up from $x = 0.9g_0$ to $x = 0.15g_0$. In fact, resistive damping alone can never damp out all the oscillations stepping back up all the way to $x = 0$ because the capacitors discharge fully leaving no voltage to drive current through the damping resistor. Hence resistive damping – simple and easy to adjust – is attractive primarily for operating the positioner in the $x > 0.5g_0$ range.

Compressible squeeze-film damping acts whenever the positioner is operated in air. It is more difficult to adjust – damping forces depend on air pressure and the geometry of the device. Fig. 8b shows the performance of the positioner under squeeze-film damping forces modeled by

$$F_d \propto \frac{dx/dt}{(g_0 - x + \lambda)^3} \tag{6.1}$$

where λ is approximately the mean free path for air [9]-[10]. In general, the larger steps (to $x \geq 0.75g_0$) are overdamped, with the approach to $x = 0.9g_0$ being almost asymptotic. This slow approach is probably overestimated by the simulation because Eq. 6.1 neglects the transition from spring-like behavior to incompressible viscous damping at lower actuation speeds. The damping at $x = 0.15g_0$ is generally much better than can be achieved with resistive damping.

Under both resistive and squeeze-film damping, the oscillations are difficult to damp out near $x = 0$. Increasing the damping forces will increase the rise time to $x = 0.9g_0$ significantly, especially for the squeeze-film damping case. Over-stabilizing the positioner i.e. making $c_1 << \frac{c_0^i}{2}$ improves the rise time for the larger steps while leaving settling times and overshoots roughly unchanged as shown in Fig. 8c. Decreasing c_1, to $\frac{c_0^i}{8}$ in this example, provides a more constant electrostatic driving force that is less dependent on the gap, especially as x approaches g_0, thus reducing asymptotic behavior. In the critically-stabilized case, the electrostatic force and the gap are more strongly interdependent and hence both approach static equilibrium asymptotically.

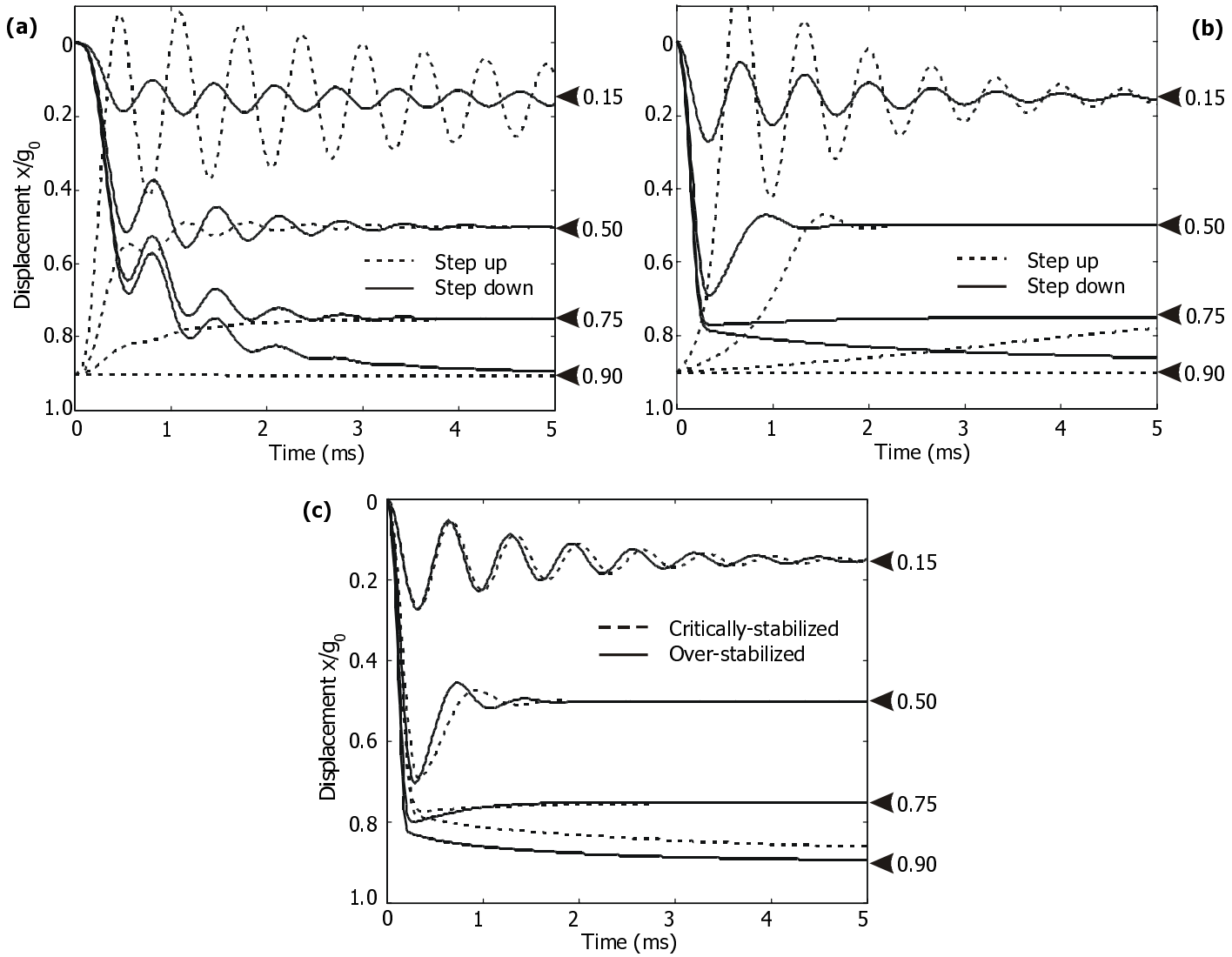

Fig. 8. (a) *Step up and step down responses of critically-stabilized positioner under resistive damping. The response is slightly overdamped for steps down to $x > 0.5g_0$ but underdamped for steps back up to $x = 0.15g_0$.* ***(b)*** *Step up and step down responses of critically-stabilized positioner under compressible squeeze-film damping. The response is severely overdamped for large steps down. The damping at small deflections (near $x=0$) is better than can be achieved using resistive damping.* ***(c)*** *Step down responses of over-stabilized positioner under squeeze-film damping compared to critically-stabilized device. The rise time is faster especially towards $x = 0.9g_0$ because the electrostatic force is less dependent on the changing gap. The damping for smaller steps is roughly unchanged.*

7. PHYSICAL DESIGN

Fig. 9a shows the straightforward three-conductor-stack implementation of the electrostatic positioner. Fabricating this device would require a dielectric layer many times the thickness of the travel gap to maintain the proper $\frac{c_0^i}{c_1}$ ratio. This device cannot be realized in MUMPs. Figs. 9a to 9d conceptualize the transformation of the initial three-conductor-stack into an equivalent two-layer design more suitable for surface micromachining. First, the floating conductor/node is extended so that the top and bottom voltage-driven electrodes can be moved apart horizontally (Fig. 9b). Then the left-hand side is "folded over" as shown in Fig. 9c. Neglecting fringing fields, the electrostatic forces acting on the movable plate, which is now below the floating electrode, are exactly the same as before. Finally, the mechanical elements on the left-hand side are swapped so that the movable electrode is once again on the top. The movable and fixed portions of the floating electrode are connected electrically. The device of Fig. 9d, which we call a "folded capacitor", is functionally equivalent to the initial design but can now be implemented in MUMPs.

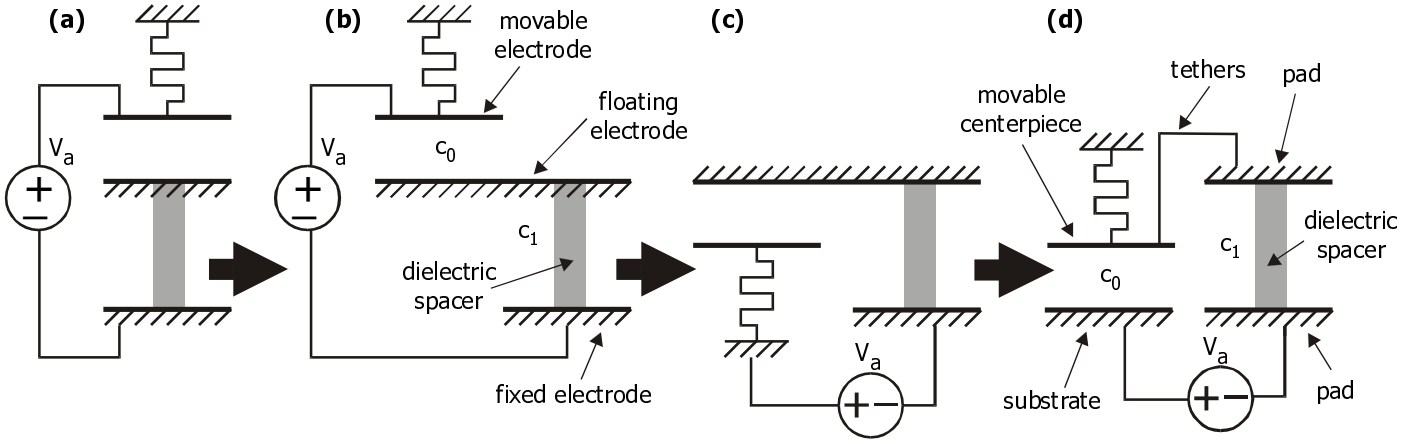

Fig. 9. *Transformation of a three-conductor-stack implementation of the electrostatic positioner into a two-layer implementation that is readily fabricated in MUMPs.* ***(a)*** *Original three-conductor vertical stack. Capacitance ratio determined by thickness (gap) ratio.* ***(b)*** *Floating electrode is extended so that fixed and movable electrodes can be separated horizontally.* ***(c)*** *The left-hand side is "folded over" so that the movable electrode is now on the bottom. Electrical connections are all on the bottom.* ***(d)*** *While the electrical connections remain unchanged, the mechanical elements on the left-hand side are swapped so that the movable electrode is once again on the top. This configuration is functionally equivalent to the configuration in (a).*

Fig. 10a is the profile of a design currently being fabricated at MCNC. The essential elements are labeled corresponding to Fig. 9d. The device consists of a nominally rigid centerpiece fabricated in POLY1 suspended by POLY2 tethers. A controlled HF etch of the sacrificial PSG creates dielectric spacers which form the capacitor c_1 and electrically-isolate the tethers and centerpiece leaving them floating. c_0 is the capacitance between the centerpiece and silicon substrate. The nitride layer prevents the shorting of the floating conductor to the silicon substrate. The POLY2 tethers are shielded from the substrate by the POLY1 centerpiece thus reducing associated parasitic capacitance. Fig. 10c is the plan view where the tethers have some meander to ensure that most of the deformation as the device is actuated occurs at the tethers leaving the centerpiece as flat as possible, mimicking 1D behavior. The flexures also provide stress relief to prevent buckling. This design, with very small parasitics and nominally flat parts, closely resembles the ideal of Fig. 9d. POLY2 is overlaid on the centerpiece to provide additional stiffness to keep the centerpiece flat. The tethers meet at the center of the POLY1 plate instead of remaining separated so that bending moments at the point of attachment to the centerpiece cancel out.

Designing for the desired $\frac{c_0^i}{c_1}$ ratio simply requires ratioing the area of the POLY1 centerpiece to the area of the POLY1 pads (attached to the PSG spacers) appropriately instead of varying layer thicknesses. The dielectric constant of the c_1 capacitors is some proportionate mixture of the dielectric constants of air and PSG that depends on the duration of the sacrificial etch. Fig. 10b is an alternate design that does not require a controlled HF etch. In this case, the nitride serves as the dielectric spacer (forming c_1) and a POLY0 pad is placed under the centerpiece (forming c_0).

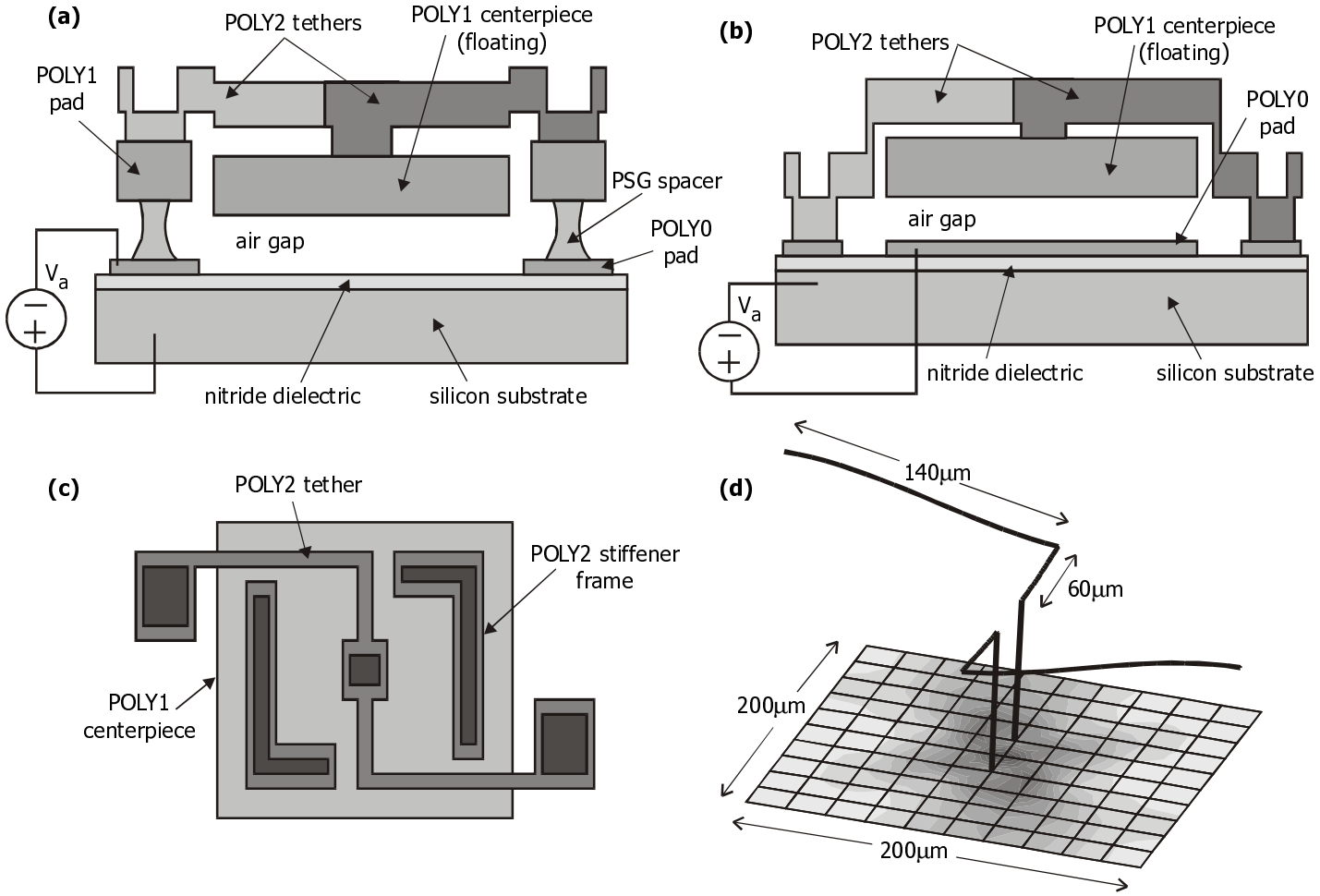

Fig. 10. (a) *Profile of electrostatic positioner being fabricated in MUMPs. The device consists of voltage-driven POLY0 pads and silicon substrate, and a POLY1 centerpiece suspended by POLY2 tethers. The tethers are shielded from the substrate by the centerpiece thus minimizing the associated parasitics. The centerpiece and tethers are electrically-isolated by the PSG spacer formed by a controlled HF sacrificial etch.* ***(b)*** *Alternate design that does not require a controlled HF etch. The nitride serves as the dielectric spacer that isolates the tethers and centerpiece. A POLY0 pad now serves as the bottom electrode to which the centerpiece is attracted.* ***(c)*** *Plan view corresponding to profile in (a). Flexures in the tethers ensure that most of the deformation during actuation occurs in the tethers thus leaving the centerpiece relatively flat. The flexures also provide stress-relief to prevent buckling. POLY2 overlaid on the POLY1 centerpiece form a stiffener frame (not shown in the profile) that further ensures that the centerpiece remains flat.* ***(d)*** *3D simulation in Abaqus using beam elements for the tethers and shell elements for the centerpiece. The stiffener frame was not modeled. At 0.6μm of average deflection, the variation across the centerpiece was less than 2%. Von Mises stress contours are shown on the centerpiece.*

Simulation results (Fig. 10d) using Abaqus with electrostatic forces imposed as user-defined loads [11]-[12] show that the design of Figs. 10a and 10c meets the requirements of flatness as detailed in Section 4. At 0.6μm of center displacement, the variation of displacement across the centerpiece is less than 2%. This flatness is desirable for optical applications such as micromechanically-tuned lasers. Decoupling the design of the tethers from the design of the centerpiece also improves the flatness of devices built for leveraged bending [4]. Figs. 11a and 11b show a proposed design that utilizes leveraging of cantilevers with widened actuation pads to position a nominally rigid and flat centerpiece. This also alleviates the need for compressively stressed materials to achieve leveraged bending.

CONCLUSION

A thorough analysis of the various practical issues involved in designing an electrostatic positioner with full-gap travel has been presented. The effects of parasitic capacitances, including the "fixed" capacitance associated with non-uniform 2D deformation, are shown along with two designs that minimize their influence – the "folded capacitor" designs employing floating electrodes suspended by shielded tethers. Residual charge simply causes a voltage shift in the response of this positioner but can be further exploited to create a linear electrostatic actuator utilizing a precharged floating conductor.

Transient damping characteristics can be improved by over-stabilizing the positioner. All devices are currently being fabricated at MCNC and measurements will be presented in an upcoming paper.

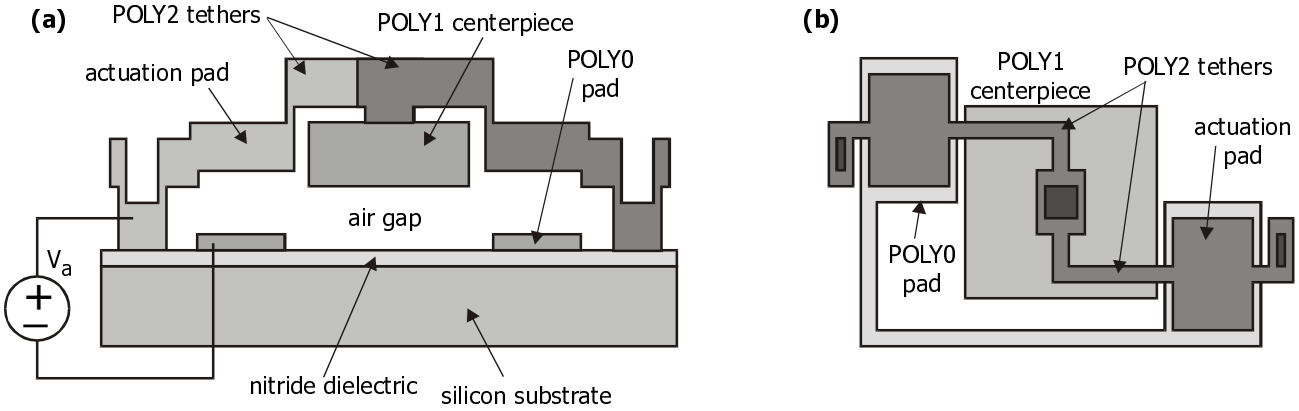

Fig. 11. *Electrostatic actuator utilizing "leveraged bending" to achieve full-gap travel exploiting the same tether design as shown in Fig. 10. Decoupling the tether design from the centerpiece allows each element to be optimized separately. The large actuation pads connected to slender beams enhance the effectiveness of leveraging.* ***(a)*** *Profile.* ***(b)*** *Plan view.*

ACKNOWLEDGEMENTS

This work was supported by the DARPA Composite CAD program (F30602-96-2-0308-P00001). The authors would like to thank B. K. Eplett and D. W. Burns for their time and valuable comments.

REFERENCES

1. C. Goldsmith, J. Randall, S. Eshelman, T. H. Lin, D. Denniston, S. Chen, B. Norvell, "Characteristics of micromachined switches at microwave frequencies," in *IEEE MTT-S International Microwave Symposium Digest*, vol. 2, San Francisco, pp. 1141-1144, June 1996.
2. C. T. -C. Nguyen, "Micromechanical resonators for oscillators and filters," in *Proceedings of IEEE Ultrasonics Symposium*, vol. 1, Seattle, pp. 489-499, November 1995.
3. E. K. Chan, K. Garikipati, R.W. Dutton, "Characterization of contact electromechanics through capacitance-voltage measurements and simulations," in *Journal of Microelectromechanical Systems* (in press).
4. E. S. Hung, S. D. Senturia, "Leveraged bending for full-gap positioning with electrostatic actuation," in *Technical Digest of Solid State Sensor and Actuator Workshop*, Hilton Head, pp. 83-86, June 1998.
5. P. B. Chu, K. S. J. Pister, "Analysis of closed-loop control of parallel plate electrostatic microgrippers," in *Proc. IEEE International Conference on Robotics and Automation*, San Diego, pp. 820-825, May 1994.
6. J. I. Seeger, S. B. Crary, "Stabilization of electrostatically actuated mechanical devices," in *Proceedings of Transducers '97*, Chicago, pp. 1133-1136, June 1997.
7. D. A. Koester, R. Mahadevan, A. Shishkoff, K. W. Markus, *SmartMUMPs Design Handbook including MUMPs Introduction and Design Rules (rev. 4)*, Microelectronics Center of North Carolina, July 1996, http://mems.mcnc.org.
8. E. K. Chan, E. C. Kan, P. M. Pinsky, R. W. Dutton, "Nonlinear dynamic modeling of micromachined microwave switches," in *IEEE MTT-S International Microwave Symposium Digest*, vol. 3, Denver, pp. 1511-1514, June 1997.
9. J. B. Starr, "Squeeze-film damping in solid-state accelerometers," in *Technical Digest of Solid State Sensor and Actuator Workshop*, Hilton Head, pp. 44-47, June 1990.
10. Y.-J. Yang, S. D. Senturia, "Numerical simulation of compressible squeezed-film damping," in *Technical Digest of Solid-State Sensor and Actuator Workshop*, Hilton Head, pp. 76-79, June 1996.
11. B. E. Artz, L. W. Cathey, "A finite element method for determining structural displacements resulting from electrostatic forces," in *Technical Digest of Solid State Sensor and Actuator Workshop*, Hilton Head, pp. 190-193, June 1992.
12. Hibbitt, Karlsson and Sorensen, Inc., *ABAQUS/Standard User's Manual*, version 5.6, Pawtucket, 1996.